

Stitching Dynamic Movement Primitives and Image-based Visual Servo Control

Ghananeel Rotithor, *Student Member, IEEE*, Iman Salehi, *Student Member, IEEE*,
Edward Tunstel, *Fellow, IEEE*, Ashwin P. Dani, *Senior Member, IEEE*

Abstract—Utilizing perception for feedback control in combination with Dynamic Movement Primitive (DMP)-based motion generation for a robot's end-effector control is a useful solution for many robotic manufacturing tasks. For instance, while performing an insertion task when the hole or the recipient part is not visible in the eye-in-hand camera, a learning-based movement primitive method can be used to generate the end-effector path. Once the recipient part is in the field of view (FOV), Image-based Visual Servo (IBVS) can be used to control the motion of the robot. Inspired by such applications, this paper presents a generalized control scheme that switches between motion generation using DMPs and IBVS control. To facilitate the design, a common state space representation for the DMP and the IBVS systems is first established. Stability analysis of the switched system using multiple Lyapunov functions shows that the state trajectories converge to a bound asymptotically. The developed method is validated by two real world experiments using the eye-in-hand configuration on a Baxter research robot.

I. INTRODUCTION

Robots are required to perform fine manipulation tasks in a variety of applications ranging from manufacturing automation to space exploration. To perform tasks involving fine manipulation, incorporating visual feedback can be beneficial when the robot end-effector is close to the object being manipulated. When the object is not in the field of view (FOV) of the camera, learning-based motion generation methods such as dynamic movement primitives (DMP) can be used to control the robot. For example, in a wire pinning task for wire harness assembly, the robot holding the wire should reach the pin by following a certain trajectory that avoids collision with the fixtures holding the pin. The pin may not always be in the FOV of the camera attached to robot end-effector. In such cases to insert the wire into the pin, a learned DMP can be used to generate the motion that takes the wire near to the pin before the visual feedback of the pin is available [1]. Motivated by such examples, a methodology that unifies DMP [2] and Image-based Visual Servoing (IBVS) [3] is proposed in this paper. The proposed algorithm switches between DMP and IBVS controllers to

reach the goal location from an initial location when the visual feedback is not continuously available.

Many approaches have been developed to design robot controllers using visual feedback that keep the objects in the FOV (see e.g., [4], [5]). A trajectory planning and tracking control approach for mobile robots is developed in [6] that uses virtual-goal-guided rapidly exploring random tree (RRT) for trajectory planning and IBVS with the FOV constraints for tracking. A constrained IBVS approach for helicopter landing on a moving platform is proposed in [7] using a control barrier function methodology to satisfy the FOV constraints. A model predictive controller (MPC) for visual servoing of a mobile robot is developed in [8] which handles visibility constraints for IBVS and velocity limits of the robot. In contrast a learning-based robot motion generation using DMP is developed in this paper to generate robot control commands in the absence of visual feedback and a switching control law is developed to switch to IBVS controller when visual feedback is available.

It is known that switching arbitrarily between stable subsystems can lead to instability [9], [10]. It is necessary to constrain the switching of such subsystems by imposing dwell time conditions in order to make the overall system stable. In [11], an average dwell time condition based on multiple Lyapunov functions is developed for stabilizing switched systems. In [12], the authors propose a linear matrix inequality-based condition to check for the existence of a quadratic Lyapunov function for proving the asymptotic stability of a switched discrete system. In [13], LaSalle's Invariance Principle is extended to switched linear systems to deduce asymptotic stability using multiple Lyapunov functions whose Lie derivatives are negative semidefinite. In [14], a survey of results for the stability of switched linear systems is presented and the problem of stabilizability of switched systems is analyzed. Multiple Lyapunov functions for analyzing Lyapunov stability and iterated function systems as a tool for Lagrange stability is proposed in [15]. Invariance-like results for nonautonomous nonlinear switched systems are developed in [16]. Switched systems analysis of output feedback systems and observers have also been studied in the literature. The switching method in [17] analyzes switching between locally and globally converging observers with asymptotic stability. A composite output feedback control law is derived in [18] that switches between locally and globally

Ghananeel Rotithor, Iman Salehi, and Ashwin P. Dani are with the Department of Electrical and Computer Engineering at University of Connecticut, Storrs, CT 06269. Email: {ghananeel.rotithor; iman.salehi; ashwin.dani}@uconn.edu. Edward Tunstel is with Raytheon Technologies, East Hartford, CT Email: tunstel@ieee.org.

asymptotically stable output feedback controllers.

Switched systems analysis has been used to solve challenging problems in robotics including visual servo control and trajectory tracking. In [19] an asymptotically stable hybrid switched systems visual servo controller is proposed which switches between IBVS and position-based visual servo control (PBVS) based on multiple Lyapunov functions. In [20], the switched systems framework is extended to achieve consensus of a distributed multi-agent system wherein the leader provides intermittent information to all the followers. In [21], the boundedness of input-to-state (ISS) stable switched systems with multiple equilibria is proven and its applications to biped locomotion are discussed. However, these results switch between systems which are either globally or locally stable. In [22], [23], an observer-predictor framework is presented for target tracking and trajectory tracking in the presence of intermittent measurements by switching between a global uniformly ultimately bounded (GUUB) and an unstable system. The switched error system is shown to be GUUB based on the dwell time conditions.

In this paper the switched systems analysis is developed for systems which are locally (IBVS) and globally (DMP) stable, and switching is occurring between image and non-image feedback. The goal is to regulate the end-effector pose with respect to a target using an eye-in-hand configuration. When the visual feedback is available, the IBVS controller is used to generate camera accelerations. When the visual feedback is not available then DMPs are used to generate camera accelerations. The DMPs are implemented as an online end-effector acceleration controller whose weights are trained using regulation task demonstration data. The contributions of this paper are as follows:

- A new IBVS acceleration control law is developed and the corresponding closed-loop dynamics are proven to be UUB if the initial state is sufficiently close to the goal state.
- Combined position and orientation DMPs are presented and the corresponding dynamics are proven to be globally asymptotically stable.
- The switching between the IBVS controller and DMP is analyzed using multiple Lyapunov functions and the switched system dynamics are proven to converge asymptotically to a bound whose analytical expression is derived. Furthermore, an algorithm is developed based on the analysis of the switched system to ensure stable switching between the IBVS and DMP subsystems.

Compared to our prior work in [24], this paper provides rigorous stability analyses for the individual DMP and IBVS systems along with an algorithm and stability analysis for the switched system. Experimental results for a pose regulation task are presented using an eye-in-hand configuration of a Baxter robot, and the switched system results are validated in the presence of occlusions in the image feedback.

The rest of the paper is organized as follows. In Section II, the coordinate frames attached to the robot base, camera

and the goal location and its kinematics are discussed. In Section III, an acceleration controller is presented for IBVS and the error dynamics are proven to be uniformly ultimately bounded (UUB). In Section IV, position and orientation DMPs are presented and global asymptotic stability of the error dynamics is presented. In Section V, the stability of the switched system is proven and an average dwell time condition is developed. Experimental results of the switched system are presented in Section VI.

Notations: The set of real numbers and integers is denoted by \mathbb{R} and \mathbb{Z} respectively. The symbols \mathbb{R}^+ and \mathbb{Z}^+ denote the set of non-negative real numbers and non-negative integers respectively. The standard Euclidean norm of a vector is denoted by $\|\cdot\|$ and for a p dimensional real vector the following set is defined $\mathcal{B}_\zeta(x) = \{x \in \mathbb{R}^p \mid \|x\| \leq \zeta\}$ where $\zeta > 0$ is a constant.

II. PROBLEM FORMULATION

Consider a fixed inertial reference frame \mathcal{F}_w and a coordinate frame \mathcal{F}_c attached to a moving camera observing a static object shown in Figure 1. The camera frame \mathcal{F}_c is bound to the camera in such a way that the Z -axis of the coordinate frame aligns with the optical axis of the camera and the X and Y axis form the basis of the image plane. Thus, the coordinate frame attached to the camera always moves along with the camera, as the camera undergoes motion. Let $R_b^a \in SO(3)$ and $t_b^a \in \mathbb{R}^3$ be the rotation and translation from a to b respectively. A quaternion representation of the rotation matrix R_b^a is given by $q_b^a \in \mathcal{S}^4$, where $\mathcal{S}^p = \{x \in \mathbb{R}^p \mid x^T x = 1\}$ is the unit hypersphere. It is assumed that the pose of the camera in the world reference frame, T_c^w is known. A coordinate frame \mathcal{F}_{c^*} is attached to the desired goal location such that when \mathcal{F}_c coincides with \mathcal{F}_{c^*} the image feature error and the pose error is zero. Additionally, the pose transformation between \mathcal{F}_w and \mathcal{F}_{c^*} , denoted as $T_{c^*}^w$, is assumed to be known. The time varying pose transformation between the current camera frame and the goal camera frame is denoted by $T_c^{c^*}(t)$ and is represented as $[(t_c^{c^*}(t))^T, (q_c^{c^*}(t))^T]^T \in \mathbb{R}^3 \times \mathcal{S}^4$.

For designing a switching control law between DMP and IBVS, a common state space between the IBVS and DMP is established. A new common auxiliary state is defined as follows

$$x(t) = [e_p^T(t) \quad \xi_{c^*}^T(t)]^T \in \mathbb{R}^{12} \quad (1)$$

where $e_p(t) = [(t_c^{c^*}(t))^T, r^T(t)]^T \in \mathbb{R}^6$ and $r(t) = 2\log(q_c^{c^*}(t)) = \Theta \mathbf{n}$ is the quaternion logarithm that transforms a quaternion into the corresponding angle-axis representation. The pose transformation $e_p(t)$ can be viewed as the pose error that indicates the deviation of the current camera frame \mathcal{F}_c from the goal camera frame \mathcal{F}_{c^*} . In (1), $\xi_{c^*}(t) = [v_{c^*}^T(t) \quad \omega_{c^*}^T(t)]^T \in \mathbb{R}^6$ is the velocity of the camera expressed in the desired frame \mathcal{F}_{c^*} , such that $v_{c^*}(t) \in \mathbb{R}^3$ is the linear velocity and $\omega_{c^*}(t) \in \mathbb{R}^3$ is the angular velocity.

Problem Description: Given the desired pose T_c^w , and the current camera pose T_c^w , the problem is to regulate the current camera frame \mathcal{F}_c to the goal camera frame \mathcal{F}_c^* using both the image feedback when it is available and a learned DMP when image feedback is not available. A stable switching controller is developed, which switches between the DMP and the IBVS control. The switching is triggered when the image features are visible in the camera FOV. The feature points may or may not be visible depending on the current camera pose. In such cases, the camera motion control is switched to DMP.

In the following sections, details of the IBVS controller and the DMP are first presented, followed by a stability analysis of the switched controller.

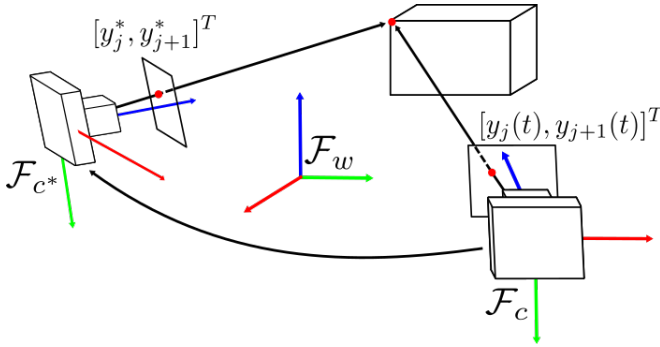


Figure 1. Reference frames attached to the camera, the goal location and the inertial reference frame.

III. IMAGE-BASED VISUAL SERVO CONTROL

The objective of IBVS is to regulate image plane feature errors to zero. Let the state vector for the current features be denoted by $s_i(t) = [y_1(t), \dots, y_{2m}(t)]^T \in \mathbb{R}^{2m}$ and let the goal feature vector be denoted by $s_i^* = [y_1^*, \dots, y_{2m}^*]^T$, where m is the number of feature points. Each feature is represented by its X and Y locations in the image plane. The dynamics of the features $s_i(t)$ can be expressed as

$$\dot{s}_i(t) = L_i(s_i, Z)\xi_c(t) \quad (2)$$

where $L_i(s_i, Z) \in \mathbb{R}^{2m \times 6}$ is the interaction matrix and $Z(t) = [Z_1(t) \dots Z_m(t)]^T \in \mathbb{R}^m$ is the time-varying depth of the feature points with respect to the camera. In (2), the vector $\xi_c(t) = [v_c^T(t) \ \omega_c^T(t)]^T$ contains the linear and angular camera velocities expressed in the camera frame \mathcal{F}_c in twist coordinates. In (2), the interaction matrix is given by $L_i(s_i, Z) = [L_{i1}^T(y_1, y_2, Z_1) \dots L_{im}^T(y_{2m-1}, y_{2m}, Z_m)]^T$ and

$$L_{ij} = \begin{bmatrix} \frac{-1}{Z_j} & 0 & \frac{y_{2j-1}}{Z_j} & y_{2j-1}y_{2j} & -(1+y_{2j-1}^2) & y_{2j} \\ 0 & \frac{-1}{Z_j} & \frac{y_{2j}}{Z_j} & 1+y_{2j}^2 & -y_{2j-1}y_{2j} & -y_{2j-1} \end{bmatrix} \quad \forall j = 1, \dots, m, \quad (3)$$

The corresponding error vector between the current and the goal image features is defined as $e_i(t) = s_i(t) - s_i^*$. The error dynamics are given by

$$\dot{e}_i(t) = L_i(s_i, Z)\xi_c(t). \quad (4)$$

Taking the time derivative of (4) yields the following second order dynamics

$$\ddot{e}_i(t) = L_i(s_i, Z)\dot{\xi}_c(t) + \dot{L}_i(s_i, \dot{s}_i, Z, \dot{Z})\xi_c(t). \quad (5)$$

Motivated by the stability analysis, the following acceleration control law is designed,

$$\dot{\xi}_c(t) = \hat{L}_i^+(s_i, Z^*) \left(-k_p e_i(t) - k_v \dot{e}_i(t) \right) \quad (6)$$

where \dot{e}_i is an approximation of \dot{e}_i which either can be computed numerically or using approximation of $Z(t)$ in (4). In this paper, the depth is approximated by the constant desired depth Z^* to construct \hat{L}_i .

Assumption 1. The approximation error $\chi(t) = \dot{e}_i(t) - \dot{\hat{e}}_i(t)$ is bounded by a constant i.e., $\exists \bar{\chi} \in [0, \infty)$ such that $\sup_{t \geq 0} \|\chi(t)\| \leq \bar{\chi}$.

In (6), $\hat{L}_i^+ = (\hat{L}_i^T \hat{L}_i)^{-1} \hat{L}_i^T$ is the pseudo-inverse of \hat{L}_i . The dependence of the variables on time and other variables is dropped in the rest of the paper unless stated. Using the relation $\dot{\hat{e}}_i(t) = \dot{e}_i(t) - \chi(t)$, and (4)-(6), the resulting closed-loop second order dynamics can be written as

$$\ddot{e}_i = -k_p L_i \hat{L}_i^+ e_i - k_v L_i \hat{L}_i^+ \dot{e}_i + \dot{L}_i \xi_c + k_v L_i \hat{L}_i^+ \chi. \quad (7)$$

To facilitate the stability analysis of the switched controller, the dynamics of the state defined in (1) is first established. To this end, a locally injective nonlinear function $\phi: \mathbb{R}^6 \rightarrow \mathbb{R}^{2m}$ which maps the pose error e_p to image error e_i using $e_i(t) = \phi(e_p(t))$ is used as described in [19], where $\phi(0) = 0$. Let $\rho(t) = [e_i^T(t) \ \dot{e}_i^T(t)]^T \in \mathbb{R}^{12}$. The following relation is obtained using the result in (4)

$$\rho = \begin{bmatrix} \phi(e_p) \\ L_i \mathbf{R} \xi_{c^*} \end{bmatrix}, \mathbf{R} = \begin{bmatrix} R_{c^*}^c & 0_{3 \times 3} \\ 0_{3 \times 3} & R_{c^*}^c \end{bmatrix} \quad (8)$$

From (8), $\rho(t) = 0$ when $x(t) = [e_p^T(t), \xi_{c^*}^T(t)]^T = 0$. Taylor series expansion of (8) at $x(t) = 0$ yields

$$\rho = \begin{bmatrix} J_1 & 0_{6 \times 6} \\ 0_{6 \times 6} & J_2 \end{bmatrix} \begin{bmatrix} e_p \\ \xi_{c^*} \end{bmatrix} + \mathcal{O} \\ \rho = \mathbf{J}x + \mathcal{O} \quad (9)$$

where $\mathbf{J} \in \mathbb{R}^{4m \times 12}$ is the Jacobian, $J_1 = \frac{\partial \phi}{\partial e_p} \big|_{e_p=0}$, $J_2 = L_i(s_i^*, Z^*) \mathbf{R}$, \mathcal{O} are the higher order terms satisfying $\mathcal{O} \leq v_1 \|x\|^2$ where $v_1 \in \mathbb{R}^+$. The Jacobian \mathbf{J} is full column rank in the neighborhood of $x(t) = 0$ as $\phi(\cdot)$ is locally injective and J_2 can be made full column rank by selecting appropriate desired feature vector $s_i^*(t)$.

As stated in Section II, to facilitate the stability analysis of the switched system, using the dynamics of $\dot{e}_p(t)$ derived in Section II B of [19], the dynamics of the common state

$x(t)$ for IBVS can now be concisely written as a first order dynamical system of the form

$$\dot{x}(t) = f_v(x(t)) + g_v(t) \quad (10)$$

where $f_v : \mathbb{R}^{12} \rightarrow \mathbb{R}^{12}$ is a locally-Lipschitz function, whose form can be derived using (9), (4) and (7) and $g_v(t) = \begin{bmatrix} 0_{1 \times 6}^T & (k_v \hat{L}_i^+ \mathbf{R}^T \chi(t))^T \end{bmatrix}^T$ is a perturbation term. To facilitate the stability analysis of the system in (10), following remarks and assumptions are stated.

Remark 1. Using the relation in (4), the upper bound on the norm of the velocity is given by $\|\xi_c\| \leq (\inf_{t \geq 0} \sigma_{\min}(L_i))^{-1} \|\dot{e}_i\|$, where $\sigma_{\min}(L_i)$ is the minimum non-zero singular value of the matrix $L_i(s_i, Z)$.

Assumption 2. The matrices $\hat{L}_i^+(s_i, Z^*)$ and $\hat{L}_i(s_i, \dot{s}_i, Z, \dot{Z})$ can be upper bounded using the constants $l_1, l_2 > 0$ as $\sup_{t \geq 0, \|\dot{e}_1\|=1} \|\hat{L}_i^+\| \leq l_1$ and $\sup_{t \geq 0, \|\dot{e}_i\|=1} \|\hat{L}_i\| \leq l_2$ in a sufficiently small neighborhood of the origin.

Remark 2. Assumption 2 is mild since it only requires $s_i(t)$, $Z(t)$ to be bounded in a local region near s_i^* (Remark 1 in [25]). The bound on the matrix $\hat{L}_i(s_i, \dot{s}_i, Z, \dot{Z})$ holds given that $s_i(t)$, $Z(t)$ are bounded, since $\dot{Z}(t)$ is a function of the bounded 3D coordinates of the feature point and the velocity vector $\xi_c(t)$ (Ch. 12 pp. 414 in [26]) which can be upper bounded using Remark 1.

Assumption 3. The matrix \hat{L}_i^+ is constructed using suitable feature points and a constant depth approximation such that in a sufficiently small neighborhood of the origin, $e_i, \dot{e}_i \notin \text{Ker}\{\hat{L}_i^+\}$, $\hat{L}_i^+ L_i > 0$ and \hat{L}_i^+ has full column rank as described in [27].

Remark 3. Assumption 2 implies that if the matrix \hat{L}_i^+ is suitably computed and the initial camera pose is in a local neighborhood of the goal camera pose, then the feature motion is realizable which ensures the final camera pose does not reach a local minimum. In this local region the matrix $\hat{L}_i^+ L_i$ is positive definite [27].

Theorem 1. If Assumptions 1 - 3 hold, then the dynamics in (10) are uniformly ultimately bounded in the sense that for an initial time $t_0 \geq 0$

$$\|x(t_0)\| < \sqrt{\frac{\gamma_v}{\gamma_v}} \delta_1 \Rightarrow \limsup_{t \rightarrow \infty} \|x(t)\| \leq \sqrt{\frac{\gamma_v}{\gamma_v} \frac{\eta}{\beta_1}} \quad (11)$$

provided that $\delta_1 > \bar{\gamma}_v / \gamma_v \sqrt{\eta / \beta_1}$ and the controller gains k_p and k_v satisfy the sufficient condition

$$\lambda_v = \lambda_{\min} \begin{bmatrix} \frac{\varepsilon_1 k_p \bar{k}}{2} & k^* \\ k^* & k_v \bar{k} - \frac{\varepsilon_1 \bar{l}}{2} \end{bmatrix} > 0 \quad (12)$$

where $k^* = -\frac{\bar{l}}{2} - \frac{\bar{k}}{2} (k_p + \frac{\varepsilon_1 k_v}{2})$ and $\varepsilon_1, \bar{k}, \bar{l}, \bar{k}, \bar{\gamma}_v, \gamma_v, \beta_1, \eta, \delta_1$ are positive constants.

Proof: Using (9), the following upper and lower bound $\underline{m}\|x\|^2 \leq \|\rho\|^2 \leq \bar{m}\|x\|^2$ can be derived where $\underline{m} = \lambda_{\min}(\mathbf{J}^T \mathbf{J})$ and $\bar{m} = \lambda_{\max}(\mathbf{J}^T \mathbf{J}) + v_1$. The operators $\lambda_{\min}(\cdot)$ and $\lambda_{\max}(\cdot)$ correspond to the minimum nonzero and maximum eigenvalues of the matrix. Consider a candidate Lyapunov function $V_v(x) : \mathcal{B}_{\delta_1}(x) \rightarrow \mathbb{R}^+$ such that $\mathcal{B}_{\delta_1}(x) \subset \mathbb{R}^{12}$

$$V_v(x) = x^T P_v x + \tilde{\mathcal{O}} = \rho^T Q \rho \quad (13)$$

with $\tilde{\mathcal{O}} \leq v_2 \|x\|^2$ indicating the higher order terms where $v_2 \in \mathbb{R}^+$. In (13), $P_v = \mathbf{J}^T Q \mathbf{J}$ and Q is expressed as

$$Q = \begin{bmatrix} \frac{1}{2} (\hat{L}_i^+)^T \hat{L}_i^+ & \frac{\varepsilon_1}{4} (\hat{L}_i^+)^T \hat{L}_i^+ \\ \frac{\varepsilon_1}{4} (\hat{L}_i^+)^T \hat{L}_i^+ & \frac{1}{2} (\hat{L}_i^+)^T \hat{L}_i^+ \end{bmatrix}, \quad (14)$$

where $\varepsilon_1 > 0$ is a suitably chosen constant. Although the matrix Q is positive semidefinite, it is known from Assumption 3 that $e_i(t), \dot{e}_i(t) \notin \text{Ker}\{\hat{L}_i^+\}$ if the initial pose of the camera is close to the goal pose, which is enough to ensure that the quadratic form in (13) is always nonzero in a local region near the origin and is zero at the origin. The Lyapunov function in (13) can be then upper and lower bounded as $\underline{\gamma}_v \|x\|^2 \leq V_v(x) \leq \bar{\gamma}_v \|x\|^2$, where $\underline{\gamma}_v = \inf_{t \geq 0} \lambda_{\min}(P_v)$ and $\bar{\gamma}_v = \sup_{t \geq 0} \lambda_{\max}(P_v) + v_2$. Taking the time derivative of (13), using (4) and (7), \dot{V}_v can be written as

$$\begin{aligned} \dot{V}_v = & e_i^T (\hat{L}_i^+)^T \hat{L}_i^+ \dot{e}_i + \dot{e}_i^T (\hat{L}_i^+)^T \hat{L}_i^+ \dot{L}_i \xi_c \\ & - k_p e_i^T (\hat{L}_i^+)^T \hat{L}_i^+ L_i \hat{L}_i^+ e_i - k_v \dot{e}_i^T (\hat{L}_i^+)^T \hat{L}_i^+ L_i \hat{L}_i^+ \dot{e}_i \\ & + k_v \dot{e}_i^T (\hat{L}_i^+)^T \hat{L}_i^+ L_i \hat{L}_i^+ \chi + \frac{\varepsilon_1}{2} \dot{e}_i^T (\hat{L}_i^+)^T \hat{L}_i^+ \dot{e}_i \\ & + \frac{\varepsilon_1}{2} e_i^T (\hat{L}_i^+)^T \hat{L}_i^+ \dot{L}_i \xi_c - \frac{\varepsilon_1 k_p}{2} e_i^T (\hat{L}_i^+)^T \hat{L}_i^+ L_i \hat{L}_i^+ e_i \\ & - \frac{\varepsilon_1 k_v}{2} e_i^T (\hat{L}_i^+)^T \hat{L}_i^+ L_i \hat{L}_i^+ \dot{e}_i \\ & + \frac{\varepsilon_1 k_v}{2} e_i^T (\hat{L}_i^+)^T \hat{L}_i^+ L_i \hat{L}_i^+ \chi \\ & + e_i^T (\hat{L}_i^+)^T \hat{L}_i^+ e_i + \dot{e}_i^T (\hat{L}_i^+)^T \hat{L}_i^+ \dot{e}_i \\ & + \frac{\varepsilon_1}{2} e_i^T (\hat{L}_i^+)^T \hat{L}_i^+ \dot{e}_i + \frac{\varepsilon_1}{2} e_i^T (\hat{L}_i^+)^T \hat{L}_i^+ \dot{e}_i \end{aligned} \quad (15)$$

Using Assumption 3, it can be ensured that $\underline{k} \|e_i\|^2 \leq e_i^T (\hat{L}_i^+)^T \hat{L}_i^+ L_i \hat{L}_i^+ e_i \leq \bar{k} \|e_i\|^2$ and $\underline{k} \|\dot{e}_i\|^2 \leq \dot{e}_i^T (\hat{L}_i^+)^T \hat{L}_i^+ L_i \hat{L}_i^+ \dot{e}_i \leq \bar{k} \|\dot{e}_i\|^2$ for some $\bar{k} \geq \underline{k} > 0$ in the local region near the origin. Using Assumption 2 and defining the following upper bounds in the considered local region as $\sup_{t \geq 0} \|(\hat{L}_i^+)^T \hat{L}_i^+\| \leq \bar{l}$, $(\inf_{t \geq 0} \sigma_{\min}\{L_i\})^{-1} \sup_{t \geq 0} \|(\hat{L}_i^+)^T \hat{L}_i^+ \dot{L}_i\| \|\dot{e}_i\| \leq \vartheta_1 \|\dot{e}_i\|^2$, $\sup_{t \geq 0} \|\hat{L}_i^+ \hat{L}_i^+\| \leq \iota \|\dot{e}_i\|$, $\bar{\varepsilon} = \max\{1, \varepsilon_1/2\}$ such that $\bar{l}, v_1, \iota > 0$. Given that the gains k_p and k_v are chosen

according to the sufficient condition in (12), then (15) can be upper bounded as

$$\begin{aligned} \dot{V}_v &\leq -\lambda_v \|e_i\|^2 - \lambda_v \|\dot{e}_i\|^2 + \bar{\varepsilon} \bar{k} k_v \bar{\chi} (\|e_i\| + \|\dot{e}_i\|) \\ &\quad + \iota \|e_i\|^2 \|\dot{e}_i\| + \frac{\varepsilon}{2} (\vartheta + 2\iota) \|e_i\| \|\dot{e}_i\|^2 + (\iota + \vartheta) \|\dot{e}_i\|^3 \end{aligned} \quad (16)$$

Using the inequality $\|e_i\| + \|\dot{e}_i\| \leq \sqrt{2(\|e_i\|^2 + \|\dot{e}_i\|^2)} = \sqrt{2}\|\rho\|$, after some algebraic manipulations and using the bounds on $\|\rho(t)\|$ and $\|x(t)\|$, (16) can be simplified to

$$\dot{V}_v \leq -\frac{\beta_1}{\gamma_v} V_v + \eta \quad (17)$$

$\forall \|\rho\| \leq \frac{\lambda_v}{2\sqrt{2}\max\{\frac{\varepsilon}{2}(\vartheta+2\iota), (\iota+\vartheta)\}}$ where $\beta_1 = \frac{\lambda_v m}{4}$ and $\eta = \frac{2m(\bar{\varepsilon} \bar{k} k_v \bar{\chi})^2}{\lambda_v m}$. The solution to the differential inequality in (17) can be obtained using the Lemma 3.4 in [28] and is given by

$$V_v(t) \leq V_v(t_0) e^{-\frac{\beta_1}{\gamma_v}(t-t_0)} + \frac{\gamma_v \eta}{\beta_1} \left(1 - e^{-\frac{\beta_1}{\gamma_v}(t-t_0)}\right) \quad (18)$$

From (18) and using the bounds on the Lyapunov function it can be concluded that $x(t) \in \mathcal{L}_\infty$. Using Theorem 4.18 in [28], the state is uniformly ultimately bounded with a bound $\limsup_{t \rightarrow \infty} \|x(t)\| \leq \sqrt{\frac{\gamma_v}{\beta_1} \eta}$ if $\|x(t_0)\| < \sqrt{\frac{\gamma_v}{\beta_1}} \delta_1$ for sufficiently small $\delta_1 > 0$ representing the local region of convergence where the linearization in (9), Assumption 2, Assumption 3 and (17) holds. ■

The ultimate bound on the state can be made arbitrarily small by adjusting the controller gains k_p, k_v and by choosing an appropriate approximation method for $\hat{e}_i(t)$ which minimizes $\bar{\chi}$.

IV. TASK SPACE DYNAMIC MOVEMENT PRIMITIVES

This section describes the position and orientation DMPs which can generate goal reaching motions while retaining the desired shape of the trajectory.

A. Combined Position and Orientation DMPs

To regulate the position and orientation error to zero, i.e., $\|e_p(t)\| \rightarrow 0$ and to retain a desired shape of the trajectory, the combined position and orientation DMPs are described by the following acceleration law

$$\tau^2 \dot{\xi}_{c^*}(t) = -\Gamma e_p(t) - \tau \Lambda \xi_{c^*}(t) + \Theta^T \Psi(z_p, z_o) \quad (19)$$

where $\xi_{c^*}(t)$ is the velocity of the camera in the frame \mathcal{F}_{c^*} , $\Gamma = \text{diag}\{(\alpha_v \beta_v) \mathbf{I}_3, (\alpha_\omega \beta_\omega) \mathbf{I}_3\}$, $\Lambda = \text{diag}\{\alpha_v \mathbf{I}_3, \alpha_\omega \mathbf{I}_3\}$ such that $\alpha_v, \alpha_\omega, \beta_v, \beta_\omega > 0$ are constant positive gains and $\tau > 0$ is the temporal scaling constant. The third term on the RHS of (19) is a nonlinear forcing function which encodes the shape of the desired trajectory, Θ and Ψ are defined as

$$\Theta = \begin{bmatrix} \theta_p & 0_{N_p \times 3} \\ 0_{N_o \times 3} & \theta_o \end{bmatrix}, \quad \Psi = \begin{bmatrix} \Psi_p(z_p) z_p(t) \\ \Psi_o(z_o) z_o(t) \end{bmatrix} \quad (20)$$

such that $\theta_p \in \mathbb{R}^{N_p \times 3}, \theta_o \in \mathbb{R}^{N_o \times 3}$ are constant weight matrices associated with the vectors of radial basis functions $\Psi_p = \left[\frac{\psi_1}{\sum_{i=1}^{N_p} \psi_i}, \dots, \frac{\psi_{N_p}}{\sum_{i=1}^{N_p} \psi_i} \right]^T \in \mathbb{R}^{N_p}$ and $\Psi_o = \left[\frac{\varphi_1}{\sum_{i=1}^{N_o} \varphi_i}, \dots, \frac{\varphi_{N_o}}{\sum_{i=1}^{N_o} \varphi_i} \right]^T \in \mathbb{R}^{N_o}$ with $N_p, N_o > 0$ as respective basis numbers. The individual basis functions are defined as $\psi_i = \exp(-h_i(z_p - c_i)^2)$ and $\varphi_i = \exp(-l_i(z_o - \nu_i)^2)$. The variables $c_i, \nu_i > 0$ are centers of the basis functions and $h_i, l_i > 0$ are the variances respectively. In (20), $z_p(t) \in \mathbb{R}$ and $z_o(t) \in \mathbb{R}$ are solutions to first order scalar differential equations given by

$$\tau \dot{z}_p(t) = -\alpha_{z_p} z_p(t), \quad \tau \dot{z}_o(t) = -\alpha_{z_o} z_o(t) \quad (21)$$

where $\alpha_{z_p}, \alpha_{z_o} > 0$ are constant positive gains.

Assumption 4. The nonlinear forcing term can be upper bounded as $\|\Theta^T \Psi\| \leq \bar{\Theta} \bar{\Psi} e^{-\underline{\alpha}(t-t_0)}$, where $\underline{\alpha} = \frac{1}{\tau} \min\{\alpha_{z_p}, \alpha_{z_o}\}$ when the DMP is active between $[t_0, t)$.

The main implication of Assumption 4 is that the Θ is bounded by a constant, i.e., $\sqrt{\lambda_{\max}(\Theta^T \Theta)} \leq \bar{\Theta}$. To facilitate the stability analysis, the initial conditions for the differential equation in (21) are set to $z_p(t_0), z_o(t_0) = 1$. Thus, based on (1), the dynamics of $\dot{e}_p(t)$ derived in Section II B of [19], and (19), the state dynamics for DMP can be concisely written as

$$\dot{x}(t) = f_d(x(t)) + g_d(t) \quad (22)$$

where $f_d : \mathbb{R}^{12} \rightarrow \mathbb{R}^{12}$ is a locally-Lipschitz function and $g_d(t) = \begin{bmatrix} 0_{1 \times 6} & (\Theta^T \Psi(z_p, z_o))^T \end{bmatrix}^T$ is a perturbation term.

B. Learning DMP Parameters

Given a demonstration trajectory with \mathcal{N} data points $\{e_p(t_k), \xi_{c^*}(t_k), \dot{\xi}_{c^*}(t_k)\}_{k=0}^{\mathcal{N}-1}$ sampled at the time instants $\{t_k\}_{k=0}^{\mathcal{N}-1}$, the DMP weights are computed by solving the following optimization problem

$$\begin{aligned} \Theta^* = \arg \min_{\Theta} \sum_{k=0}^{\mathcal{N}-1} &\left\| \tau^2 \dot{\xi}_{c^*}(t_k) + \Gamma e_p(t_k) + \tau \Lambda \xi_{c^*}(t_k) \right. \\ &\left. - \Theta^T \Psi(z_p(t_k), z_o(t_k)) \right\|^2 \end{aligned} \quad (23)$$

for suitably chosen values of τ, Γ and Λ . The centers and variances are calculated as $c_i = e^{-\alpha_{z_p}(\frac{i-1}{N_p-1})}$, $h_i = \frac{1}{(c_{i+1} - c_i)^2}$, $h_{N_p} = h_{N_p-1}$, $\forall i = 1, \dots, N_p$ and $\nu_j = e^{-\alpha_{z_o}(\frac{j-1}{N_o-1})}$, $l_j = \frac{1}{(\nu_{j+1} - \nu_j)^2}$, $l_{N_o} = l_{N_o-1}$, $\forall j = 1, \dots, N_o$.

C. Stability Analysis of DMPs

This subsection presents the stability analysis of the DMP described in Section IV-A.

Property 1. [29] Based on the definition of $r(t)$ defined after (1), the following relations hold,

$$r^T(t) \dot{r}(t) = r^T(t) \omega_{c^*}(t), \quad \dot{r}^T(t) \omega_{c^*}(t) = \omega_{c^*}^T(t) \omega_{c^*}(t). \quad (24)$$

Theorem 2. Provided that Assumption 4 holds, then the system in (22) is globally asymptotically stable in the sense that

$$\lim_{t \rightarrow \infty} \|x(t)\| = 0 \quad (25)$$

given that the gains α_v , β_v , α_ω and β_ω are chosen according to the sufficient condition

$$\alpha_v = 4\beta_v, \alpha_\omega = 4\beta_\omega, \beta_v > \frac{3\varepsilon_2}{8\tau}, \beta_\omega > \frac{3\varepsilon_2}{8\tau} \quad (26)$$

where ε_2 is a positive constant.

Proof: Consider the candidate Lyapunov function $V_d(x) : \mathbb{R}^{12} \rightarrow \mathbb{R}^+$ defined as

$$V_d(x) = x^T P_d x \quad (27)$$

where $P_d = \begin{bmatrix} \frac{1}{2}\Gamma & \frac{\varepsilon_2}{4}\mathbf{I}_6 \\ \frac{\varepsilon_2}{4}\mathbf{I}_6 & \frac{\tau}{2}\mathbf{I}_6 \end{bmatrix}$. The Lyapunov function in (27) is upper and lower bounded as $\underline{\gamma}_d \|x\|^2 \leq V_d(x) \leq \overline{\gamma}_d \|x\|^2$, where $\underline{\gamma}_d = \lambda_{\min}(P_d)$ and $\overline{\gamma}_d = \lambda_{\max}(P_d)$. Taking the time derivative of $V_d(x)$, using the definition of $x(t)$ in (1), substituting (24), (19), and simplifying yields

$$\begin{aligned} \dot{V}_d = & -\tau \xi_{c^*}^T \Lambda \xi_{c^*} + \xi_{c^*}^T \Theta^T \Psi - \frac{\varepsilon_2}{2\tau^2} e_p^T \Gamma e_p - \frac{\varepsilon_2}{2\tau} e_p^T \Lambda \xi_{c^*} \\ & + \frac{\varepsilon_2}{2\tau^2} e_p^T \Theta^T \Psi + \frac{\varepsilon_2}{2} \xi_{c^*}^T \xi_{c^*} \end{aligned} \quad (28)$$

The DMP gain relations are selected as per [30] to be $\alpha_v = 4\beta_v$ and $\alpha_\omega = 4\beta_\omega$ to make a proportional-derivative like part of the system critically damped. Defining the constants $\bar{c}_1 \geq \frac{\varepsilon_2 \Theta \Psi}{2\tau^2}$, $\bar{c}_2 \geq \frac{2\tau \bar{c}_1}{\varepsilon_2}$, $C = \max\{\bar{c}_1, \bar{c}_2\}$, if β_v and β_ω are chosen according to the sufficient conditions in (26), then (28) can be upper bounded as $\dot{V}_d \leq -\lambda_d \|x\|^2 + \sqrt{2} C e^{-\alpha(t-t_0)} \|x\|$ where $\lambda_d = \min\left\{\frac{\varepsilon_2 \beta_v^2}{\tau^2}, 4\tau\beta_v - \frac{3\varepsilon_2}{2}, \frac{\varepsilon_2 \beta_\omega^2}{\tau^2}, 4\tau\beta_\omega - \frac{3\varepsilon_2}{2}\right\}$. Completing squares and using the bounds on the Lyapunov function yields

$$\begin{aligned} \dot{V}_d & \leq -\frac{\lambda_d}{2\overline{\gamma}_d} V_d + \frac{C^2}{\lambda_d} e^{-2\alpha(t-t_0)} \\ & \leq -\beta_2 V_d + \varpi e^{-2\alpha(t-t_0)} \end{aligned} \quad (29)$$

where $\beta_2 = \frac{\lambda_d}{2\overline{\gamma}_d}$, $\varpi = \frac{C^2}{\lambda_d^2}$. The solution to the differential inequality in (29) can be obtained using Lemma 3.4 in [28] as

$$V_d(t) \leq V_d(t_0) e^{-\beta_2(t-t_0)} + \bar{\varrho} e^{-c_2(t-t_0)} \quad (30)$$

where $c_2 = \min\{2\alpha, \beta_2\}$ and $\bar{\varrho} = \frac{\varpi}{|\beta_2 - 2\alpha|}$ such that $|\cdot|$ denotes the absolute value of the argument. Using (30) and the bounds on the Lyapunov function, it can be concluded that $\|x(t)\| \in \mathcal{L}_\infty$. The second term on the right hand side of (29) is a non-negative continuous perturbation term which satisfies $\lim_{t \rightarrow \infty} \varpi e^{-2\alpha(t-t_0)} = 0$ resulting in the global asymptotic stability of the solution trajectories $x(t)$ (c.f. Lemma 9.6 in [28]). ■

V. STABILITY ANALYSIS OF THE SWITCHED SYSTEM

In this section, the stability of switched system is analyzed while switching between DMP and IBVS controllers. To facilitate the stability analysis the common state defined in (1) and stability results, which are derived for the dynamics of the common state using IBVS control and DMP, are used. The switched system switches between the IBVS controller in (6) and DMP in (19) based on the visibility of feature points. The switching between the controllers leads to discontinuous dynamics which can be mathematically expressed as

$$\dot{x}(t) = f_{\sigma(t)}(x(t)) + g_{\sigma(t)}(t) \quad \sigma(\cdot) : [0, \infty) \rightarrow q \in \{v, d\}. \quad (31)$$

The switching signal $\sigma(t)$ governs the dynamics of $x(t)$. Since the IBVS exponentially converges to a bound when initialized in a local region near the goal state, a threshold constant $\delta_2 > 0$ is selected for the IBVS controller to be active such that, $x(t) \in \mathcal{B}_{\delta_2}(x) \subset \mathcal{B}_{\delta_1}(x)$. The relation between the positive constants δ_1 and δ_2 is established using the analysis in Theorem 3.

Remark 4. In practice, a threshold for image pixel error $e_i(t)$ and velocity $\xi_{c^*}(t)$ which corresponds to δ_2 can be chosen based on the image size and feature visibility. The IBVS system is active when all the features are detected, matched and $-\iota \leq e_i \leq \iota$ for some suitably chosen vector $\iota > 0_{2m \times 1}$. No threshold is selected for the velocities $\xi_{c^*}(t)$, however, the constant τ in (19) can be adjusted to generate slow velocities using the DMP.

Let $\bar{\kappa} = \max\{\overline{\gamma}_v, \overline{\gamma}_d\}$, $\underline{\kappa} = \min\{\underline{\gamma}_v, \underline{\gamma}_d\}$, $\mu = \frac{\bar{\kappa}}{\underline{\kappa}}$ be constants. The Lyapunov functions V_v and V_d in (13) and (27) can then be related as follows.

$$V_v(x) \leq \mu V_d(x), \quad V_d(x) \leq \mu V_v(x) \quad \forall x(t) \in \mathcal{B}_{\delta_1}(x). \quad (32)$$

Definition 1. (Ch. 3, pp. 58 in [9]) The switching signal $\sigma(t)$ has average dwell time τ_a , if there exist two numbers $N_0 \in \mathbb{Z}^+$ and $\tau_a \in \mathbb{R}^+$ such that

$$N_\sigma(t, \underline{t}) \leq N_0 + \frac{t - \underline{t}}{\tau_a} \quad (33)$$

is satisfied, where N_0 is known as the chatter bound and $N_\sigma(t, \underline{t})$ are the number of discontinuities on the interval $[\underline{t}, t)$.

Theorem 3. Provided that Assumptions 1 - 4 hold, the state trajectories of the switched system generated by the family of subsystems described by (31) and a piecewise constant, right continuous switching signal $\sigma(\cdot) : [0, \infty) \rightarrow q \in \{v, d\}$ asymptotically converge to a bound in the sense that

$$\limsup_{t \rightarrow \infty} \|x(t)\| \leq \sqrt{\frac{\bar{\kappa}^{N_0+1} b}{\underline{\kappa}^{N_0+2} \epsilon}} \quad (34)$$

provided that

$$\text{I If } x(t) \in \mathbb{R}^{12} \setminus \mathcal{B}_{\delta_2}(x) \Rightarrow \sigma(t) = d.$$

II The local region of convergence and the switching threshold satisfy the following condition

$$\sqrt{\frac{\underline{\kappa}}{\bar{\kappa}}} \delta_1 > \delta_2 > \sqrt{\frac{\bar{\kappa}^{N_0+1} b}{\underline{\kappa}^{N_0+2} \epsilon}}. \quad (35)$$

III The condition in (33) is satisfied for

$$\tau_a > \frac{\ln \mu}{\underline{\beta} - \epsilon} \quad (36)$$

where $0 < \epsilon < \underline{\beta} \leq \min \left\{ \frac{\beta_1}{\gamma_v}, c_2 \right\}$ and $b = \frac{\eta}{\beta_1}$.

Proof: The proof of the theorem is divided into two cases to characterize the behavior of the switched system in different regions of the space. Consider the Lyapunov function defined in (13) and (27)

$$V_{\sigma(t)} = \begin{cases} x^T P_v x + \tilde{O} & \sigma(t) = v \\ x^T P_d x & \sigma(t) = d \end{cases} \quad (37)$$

Case 1. When $\|x(t)\| > \delta_2$, the state $x(t) \in \mathbb{R}^{12} \setminus \mathcal{B}_{\delta_2}(x)$ is outside of the switching set for IBVS. If Condition I of Theorem 3 is satisfied, then $V_{\sigma(t)}(x(t))$ decreases exponentially from any initial condition. Let $t_0 > 0$ be the first time instance when $\|x(t)\| \leq \delta_2$. Then $\forall t \in [0, t_0)$ the following upper bound holds

$$\begin{aligned} V_{\sigma(t)}(t) &\leq V_{\sigma(0)}(0) e^{-\beta_2 t} + \bar{\varrho} e^{-c_2 t} \quad \sigma(\cdot) : [0, t_0) \rightarrow d \\ &\leq (V_{\sigma(0)}(0) + \bar{\varrho}) e^{-\underline{\beta} t} \end{aligned} \quad (38)$$

The controller switches to IBVS when $\|x(t_0)\| \leq \delta_2$. To ensure that switched system state trajectories remain in a strict closed subset of the local region, i.e., $\|x(t_0)\| \leq \delta_2 \Rightarrow \|x(t)\| < \delta_1$, it can be concluded that the threshold pose constant must satisfy the relation $\delta_2 < \sqrt{\frac{\underline{\kappa}}{\bar{\kappa}}} \delta_1$. The time required to reach the set $\mathcal{B}_{\delta_2}(x)$ from any initial condition can be lower bounded by $t_0 \geq \frac{1}{\underline{\beta}} \ln \left(\min \left\{ \frac{\gamma_d \|x(t_0)\|^2 + \bar{\varrho}}{\gamma_d \delta_2^2}, 1 \right\} \right)$.

Case 2. Let the system switch to the IBVS controller for the first time at time t_0 when $\|x(t_0)\| \leq \delta_2$ implying that $x(t_0) \in \mathcal{B}_{\delta_2}(x)$. Using a recursion similar to the results in [31], Lyapunov bounds in (18), (30), and the average dwell time condition in (33) and (36), the conservative bound on the solution of the Lyapunov function in (37) between the interval $[t_0, t)$ can be given as

$$\begin{aligned} V_{\sigma(t)}(t) &\leq \mu^{N_0+1} \left((V_{\sigma(t_0)}(t_0) + (N_{\sigma(t,t_0)} + 1) \bar{\varrho}) e^{-\epsilon(t-t_0)} \right. \\ &\quad \left. + \frac{\eta}{\beta_1 \epsilon} (1 - e^{-\epsilon(t-t_0)}) \right), \quad \forall x(t) \in \mathcal{B}_{\delta_1}(x) \end{aligned} \quad (39)$$

Given that $N_{\sigma(\infty, t_0)}$ is finite, it can be concluded from (39) that $x(t)$ is continuous, $x(t) \in \mathcal{L}_\infty$ and converges asymptotically to a bound in the sense that $\limsup_{t \rightarrow \infty} \|x(t)\| \leq$

$$\sqrt{\frac{\bar{\kappa}^{N_0+1} b}{\underline{\kappa}^{N_0+2} \epsilon}}.$$

The bound on the switched system is conservative compared to the bound on the individual IBVS system as switching between subsystems can lead to growth of the Lyapunov

Algorithm 1: Algorithm for switching between IBVS and DMP based on visibility of feature points and average dwell time condition

Select decay rates $\beta, \epsilon > 0$, chatter bound $N_0 \geq 1$, feature error thresholds $\bar{\iota} > \underline{\iota} > 0_{2m}$;
 Compute $\mu = \frac{\bar{\kappa}}{\underline{\kappa}}$ and $\tau_a = \frac{\ln \mu}{\underline{\beta} - \epsilon}$;
 Set $t_d = 0$ and $t_v = 0$ to be the last time instant when DMP and IBVS were active respectively;
 Set $t_e = 0$ as the elapsed time and $\bar{N} > 1$ as the number of switches over the dwell time condition that should be satisfied;
 Set the compensation time $t_c = 0$ and current number of switches $N_\sigma = 0$;
while data is available **do**
 if features match & $-\iota \leq e_i \leq \iota$ & $t > t_v + t_c$
 then
 Run IBVS in (6);
 if $t_d > t_v$ **then**
 $t_e \leftarrow t_e + (t_d - t_v)$;
 $N_\sigma \leftarrow N_\sigma + 1$;
 $t_c \leftarrow 0$;
 $\iota \leftarrow \bar{\iota}$;
 $t_v \leftarrow t$;
 else
 Run DMP in (19);
 if $t_v > t_d$ **then**
 $N_\sigma \leftarrow N_\sigma + 1$;
 $t_e \leftarrow t_e + (t_v - t_d)$;
 if $N_\sigma = \bar{N}$ **then**
 $t_c \leftarrow (N_\sigma - N_0) \tau_a - t_e$;
 $t_e \leftarrow 0$;
 $N_\sigma \leftarrow 0$;
 $\iota \leftarrow \underline{\iota}$;
 $t_d \leftarrow t$;
 end
 end
end

function. Such a bound is commonly found in the literature in different contexts (c.f. Theorem 1 in [32], Lemma 2 in [21], Theorem 1 in [33]).

Remark 5. Theorem 3 establishes the general conditions for switching between the considered subsystems and is useful in the case of frequent perturbations or occlusions which can result in fast switching making the combined system unstable if the average dwell time condition is not satisfied.

Remark 6. Algorithm 1 is developed based on the stability analysis presented in Theorem 3 to ensure stable switching by compensating for the fast switching occurring due to the disturbances and occlusions in the IBVS subsystem. A compensation time t_c is calculated and the DMP subsystem is kept active for additional time to ensure that the average dwell time condition is satisfied for a total of $\bar{N} > 0$ switches.

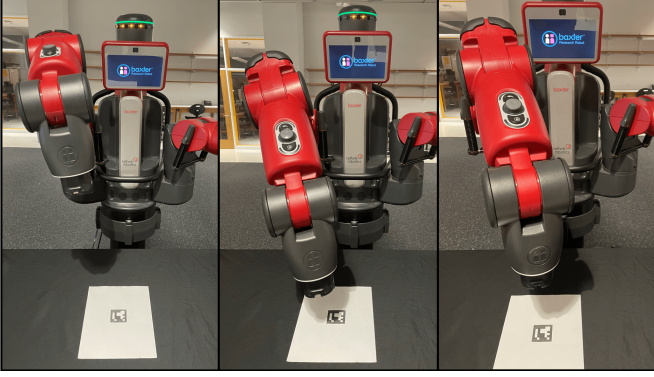


Figure 2. The experimental setup showing Baxter's end-effector with an eye-in-hand configuration observing the ArUco marker while moving from an initial camera pose (left-most picture) to the desired camera pose (right-most picture).

VI. EXPERIMENTS

A. Experimental Setup

The camera in the wrist of the right arm of a Baxter research robot is used to capture images containing an ArUco marker at a rate of 30 fps with resolution 640×420 . The corners of the ArUco marker are used as feature points ($m = 4$). The feature points are detected and matched using OpenCV's ArUco library. The processing is done at 30 fps using a desktop with an Intel Core2Duo CPU with clock-speed of 2.26 GHz and 4 GB RAM running Ubuntu 14.04. The experimental setup is shown in Figure 2. The DMP, IBVS and switching algorithms are implemented in MATLAB 2018a. The camera intrinsics for Baxter's right hand camera obtained through the Baxter API and Robot Operating System (ROS) are given by $f_x = f_y = 407.1$, $c_x = 323.4$ and $c_y = 205.6$ where f_x, f_y represent the camera focal lengths in pixels and (c_x, c_y) represents the camera center pixel.

The position DMP is trained on a demonstration trajectory collected by recording Baxter's right arm position, velocity and acceleration are filtered using a constant acceleration Kalman filter. The orientation DMP is trained on a trajectory generated by a minimum-jerk polynomial for quaternions. The goal pose of the DMP is used to record the desired feature vector s_i^* . Although the DMPs can be efficiently used to generate position or velocity commands of the robot end-effector, in this paper the DMP acceleration commands are computed from the Baxter robot pose feedback. The IBVS and DMP controller-generated acceleration is integrated and applied as a joint space velocity controller using the pseudoinverse of the Baxter manipulator Jacobian matrix.

B. Experiment 1

The convergence and stability of the switched IBVS and DMP system is verified using a single switching instance. The DMP parameters are computed by recording a single trajectory as described earlier. The DMP parameters are set

to $\alpha_v = 140$, $\beta_v = 35$, $\alpha_\omega = 4$, $\beta_\omega = 1$, $\alpha_{z_p} = 1$, $\alpha_{z_o} = 1$ and $\tau = 25$. The IBVS gains are experimentally tuned to be $k_p = 5$ and $k_v = 10$. The initial pose of the Baxter right-hand camera is chosen such that none of the desired feature points are in the FOV of the camera. The feature threshold error for switching is chosen as $\underline{\epsilon} = [0.42 \dots 0.42]$ which corresponds to pixel errors of 175 pixels and $\bar{\epsilon} = [0.85 \dots 0.85]$ corresponding to pixel errors of 350 pixels. When the features are out of the FOV the arm starts approaching the goal location along the desired DMP trajectory. Once the features are in the FOV of the camera and the feature threshold error is less than the selected feature threshold error i.e $-\underline{\epsilon} \leq e_i \leq \bar{\epsilon}$, the control switches to IBVS. This condition is first satisfied at $t = 16.4$ s. The results of experiment are summarized in Figure 3(a)-(d). Figure 3(a) shows the acceleration control generated by the IBVS and DMP controllers with the discontinuity seen at the switching instant. The pose error $e_p(t)$ is seen in Figure 3(b) and converges to a bound with the IBVS controller active after $t = 16.4$ s. Figure 3(c) shows the image feature error $e_i(t)$, which is first computed when all the features are visible and the error decreases exponentially to a bound as the switched system converges. Figure 3(d) shows the Lyapunov function $V_{\sigma(t)}(x(t))$ for the switched system. The Lyapunov function exponentially decreases for both controllers verifying the result of Theorem 3.

C. Experiment 2

In the second experiment, the case when the feature points are occluded frequently is considered. The features are occluded using a piece of paper covering the camera view. To implement Algorithm 1, the constant $\mu = 10.67$ is used. The values for the decay rates $\underline{\beta} = 0.77$ and $\epsilon = 0.01\underline{\beta}$ are chosen experimentally based on the decay rates of the individual subsystems. The value of the average dwell time is calculated as $\tau_a = 13.82$ s. The individual DMP and IBVS parameter are the same as those from Experiment 1. The constants are selected as $\bar{N} = 4$ and $N_0 = 1$, which allows the total time between \bar{N} switches to be $3\tau_a$ thus allowing the average dwell time to be relaxed to 10.36 s. This also implies that if the first 3 switches between IBVS and DMP controllers are fast, then Algorithm 1 ensures that the average dwell time condition is met by keeping the DMP controller active for longer time before the 4th switch occurs. The results of Experiment 2 are summarized in Figures 4(a)-(d). Figure 4(a) shows the acceleration generated by the switched systems with the switching instants marked with grey dashed-dotted lines. The switching occurs at the following time instances $t = 15.56$ s, $t = 16.44$ s, $t = 19.12$ s, $t = 21.48$ s and $t = 57.08$ s. It can be also seen that after the initial 3 fast switches, Algorithm 1 ensures the average dwell time condition is met by keeping the DMP system active between $t = 21.48 - 57.08$ s. Figure 4(b) shows the convergence of the pose error to a bound. Figure 4(c) shows the exponential decay of the image feature errors when the IBVS controller

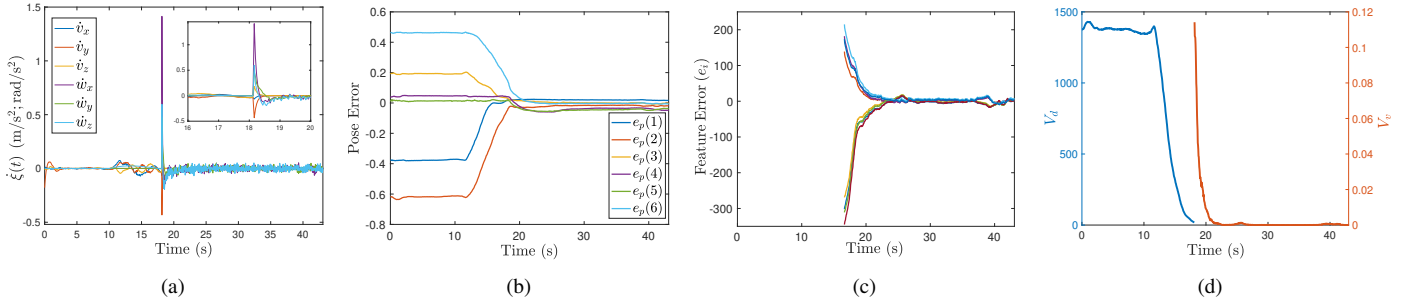


Figure 3. Simulation results for the DMP and IBVS for a single switching instance at 16.4 s. (a) Camera acceleration generated by DMP controller till 16.4 s and camera acceleration generated by IBVS controller after 16.4 s. (b) Pose error $e_p(t)$ converges to a bound. (c) Image feature errors $e_i(t)$ computed after 16.4 s. (d) Value of Lyapunov function $V_{\sigma(t)}(x(t))$, with left y-axis showing the scale for $V_d(x(t))$ and right y-axis showing the scale for $V_v(x(t))$.

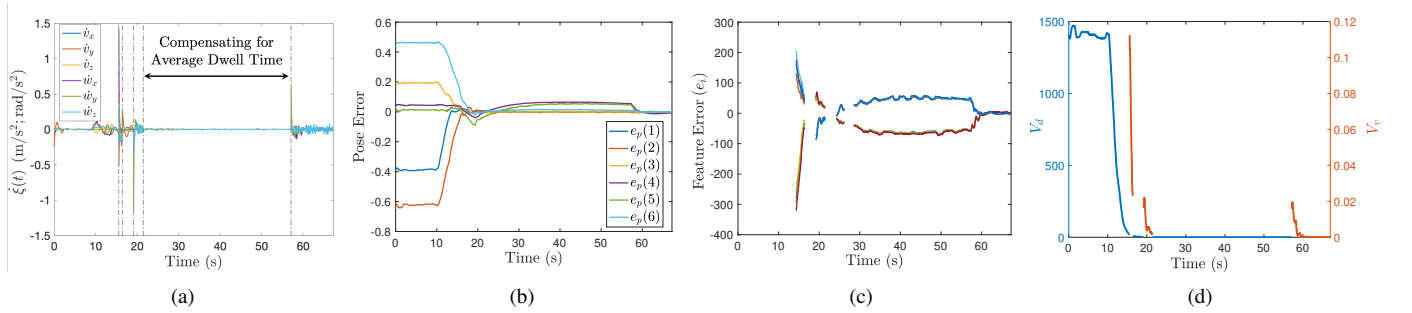


Figure 4. Simulation results for the DMP and IBVS with frequent feature occlusion (a) Camera acceleration generated by DMP controller and the IBVS controller in the presence of occlusion with grey 'dashed-dotted lines' showing the switching instances. (b) Pose error $e_p(t)$ converges to a bound in the presence of multiple switching instances. (c) Image feature errors $e_i(t)$ computed when all the features are visible and satisfy the threshold condition in Algorithm 1. (d) Value of Lyapunov function $V_{\sigma(t)}(x(t))$ during multiple switching instances, with left y-axis showing the scale for $V_d(x(t))$ and right y-axis showing the scale for $V_v(x(t))$.

is active. It can be seen that, although all the features are visible and the feature error is below the selected threshold, the DMP controller is active between $t = 21.48 - 57.08$ s to compensate for the average dwell time. Figure 4(d) shows the asymptotic stability of the Lyapunov function $V_{\sigma(t)}(x(t))$ for the switched system.

VII. CONCLUSION

In this paper a switching strategy that utilizes DMP and IBVS methodologies to combine end-effector control and perception-based control is presented. The Lyapunov stability analysis of the proposed IBVS system yields a UUB result in a local region around the origin, and that of DMP system yields global asymptotic stability. The switched DMP-IBVS system analysis based on multiple Lyapunov functions shows that the switched system asymptotically converges to a bound. A switching algorithm is presented based on feature visibility while maintaining stability in the sense of an average dwell time condition. The method is tested on a Baxter research robot using a pose regulation task of the robot's end-effector over an ArUco marker placed on a table. Future work will involve applying the developed method in various manufacturing and space robotics applications.

REFERENCES

- [1] E. Tunstel, A. Dani, C. Martinez, B. Blakeslee, J. Mendoza, R. Saltus, D. Trombetta, G. Rotithor, T. Fuhlbrügge, D. Lasko, and J. Wang, "Robotic wire pinning for wire harness assembly automation," in *2020 IEEE/ASME International Conference on Advanced Intelligent Mechatronics (AIM)*, 2020, pp. 1208–1215.
- [2] A. J. Ijspeert, J. Nakanishi, and S. Schaal, "Learning attractor landscapes for learning motor primitives," in *Advances in Neural Information Processing Systems*, 2003, pp. 1547–1554.
- [3] F. Chaumette and S. Hutchinson, "Visual servo control. I. basic approaches," *IEEE Robotics & Automation Magazine*, vol. 13, no. 4, pp. 82–90, 2006.
- [4] G. López-Nicolás, N. R. Gans, S. Bhattacharya, C. Sagüés, J. J. Guerrero, and S. Hutchinson, "Homography-based control scheme for mobile robots with nonholonomic and field-of-view constraints," *IEEE Transactions on Systems, Man, and Cybernetics, Part B (Cybernetics)*, vol. 40, no. 4, pp. 1115–1127, 2009.
- [5] N. R. Gans, G. Hu, K. Nagarajan, and W. E. Dixon, "Keeping multiple moving targets in the field-of-view of a mobile camera," *IEEE Transactions on Robotics*, vol. 27, no. 4, pp. 822–828, 2011.
- [6] R. Wang, X. Zhang, Y. Fang, and B. Li, "Virtual-goal-guided RRT for visual servoing of mobile robots with FOV constraint," *IEEE Transactions on Systems, Man, and Cybernetics: Systems*, pp. 1–11, 2021.
- [7] Y. Huang, M. Zhu, Z. Zheng, and K. H. Low, "Linear velocity-free visual servoing control for unmanned helicopter landing on a ship with visibility constraint," *IEEE Transactions on Systems, Man, and Cybernetics: Systems*, pp. 1–15, 2021.
- [8] F. Ke, Z. Li, H. Xiao, and X. Zhang, "Visual servoing of constrained mobile robots based on model predictive control," *IEEE Transactions on Systems, Man, and Cybernetics: Systems*, vol. 47, no. 7, pp. 1428–1438, 2017.

- [9] D. Liberzon, *Switching in systems and control*. Springer Science & Business Media, 2003.
- [10] D. Liberzon and A. S. Morse, “Basic problems in stability and design of switched systems,” *IEEE Control Systems Magazine*, vol. 19, no. 5, pp. 59–70, 1999.
- [11] J. P. Hespanha and A. S. Morse, “Stability of switched systems with average dwell-time,” in *Proceedings of the 38th IEEE Conference on Decision and Control*, vol. 3, 1999, pp. 2655–2660.
- [12] J. Daafouz, P. Riedinger, and C. Jung, “Stability analysis and control synthesis for switched systems: a switched Lyapunov function approach,” *IEEE Transactions on Automatic Control*, vol. 47, no. 11, pp. 1883–1887, 2002.
- [13] J. P. Hespanha, “Uniform stability of switched linear systems: Extensions of LaSalle’s invariance principle,” *IEEE Transactions on Automatic Control*, vol. 49, no. 4, pp. 470–482, 2004.
- [14] H. Lin and P. J. Antsaklis, “Stability and stabilizability of switched linear systems: a survey of recent results,” *IEEE Transactions on Automatic Control*, vol. 54, no. 2, pp. 308–322, 2009.
- [15] M. S. Branicky, “Multiple Lyapunov functions and other analysis tools for switched and hybrid systems,” *IEEE Transactions on Automatic Control*, vol. 43, no. 4, pp. 475–482, 1998.
- [16] R. Kamalapurkar, J. A. Rosenfeld, A. Parikh, A. R. Teel, and W. E. Dixon, “Invariance-like results for nonautonomous switched systems,” *IEEE Transactions on Automatic Control*, vol. 64, no. 2, pp. 614–627, 2018.
- [17] D. Astolfi, R. Postoyan, and D. Nesic, “Uniting observers,” *IEEE Transactions on Automatic Control*, vol. 65, no. 7, pp. 2867–2882, 2020.
- [18] C. Prieur and A. R. Teel, “Uniting local and global output feedback controllers,” *IEEE Transactions on Automatic Control*, vol. 56, no. 7, pp. 1636–1649, 2011.
- [19] N. R. Gans and S. A. Hutchinson, “Stable visual servoing through hybrid switched-system control,” *IEEE Transactions on Robotics*, vol. 23, no. 3, pp. 530–540, 2007.
- [20] H.-Y. Chen, Z. I. Bell, P. Deptula, and W. E. Dixon, “A switched systems framework for path following with intermittent state feedback,” *IEEE Control Systems Letters*, vol. 2, no. 4, pp. 749–754, 2018.
- [21] S. Veer and I. Poulakakis, “Switched systems with multiple equilibria under disturbances: Boundedness and practical stability,” *IEEE Transactions on Automatic Control*, vol. 65, no. 6, pp. 2371–2386, 2020.
- [22] A. Parikh, T.-H. Cheng, R. Licitra, and W. E. Dixon, “A switched systems approach to image-based localization of targets that temporarily leave the camera field of view,” *IEEE Transactions on Control Systems Technology*, vol. 26, no. 6, pp. 2149–2156, 2017.
- [23] H. Chen, Z. I. Bell, P. Deptula, and W. E. Dixon, “A switched systems approach to path following with intermittent state feedback,” *IEEE Transactions on Robotics*, vol. 35, no. 3, pp. 725–733, 2019.
- [24] G. Rotithor and A. P. Dani, “Combining motion primitives and image-based visual servo control,” in *International Symposium on Flexible Automation*. American Society of Mechanical Engineers, 2020.
- [25] G. Rotithor, D. Trombetta, R. Kamalapurkar, and A. P. Dani, “Full- and reduced-order observers for image-based depth estimation using concurrent learning,” *IEEE Transactions on Control Systems Technology*, pp. 1–7, 2020.
- [26] M. W. Spong, S. Hutchinson, and M. Vidyasagar, *Robot modeling and control*. Wiley New York, 2006, vol. 3.
- [27] F. Chaumette, “Potential problems of stability and convergence in image-based and position-based visual servoing,” in *The Confluence of Vision and Control*. Springer, 1998, pp. 66–78.
- [28] H. K. Khalil, *Nonlinear Systems*, 3rd ed. Prentice Hall, 2002.
- [29] D. Han, Q. Wei, Z. Li, and W. Sun, “Control of oriented mechanical systems: A method based on dual quaternion,” *IFAC Proceedings Volumes*, vol. 41, no. 2, pp. 3836–3841, 2008.
- [30] A. Ude, B. Nemec, T. Petrić, and J. Morimoto, “Orientation in Cartesian space dynamic movement primitives,” in *2014 IEEE International Conference on Robotics and Automation (ICRA)*. IEEE, 2014, pp. 2997–3004.
- [31] L. Vu, D. Chatterjee, and D. Liberzon, “Input-to-state stability of switched systems and switching adaptive control,” *Automatica*, vol. 43, no. 4, pp. 639–646, 2007.
- [32] J. R. Klotz, A. Parikh, T. Cheng, and W. E. Dixon, “Decentralized synchronization of uncertain nonlinear systems with a reputation algorithm,” *IEEE Transactions on Control of Network Systems*, vol. 5, no. 1, pp. 434–445, 2018.
- [33] J. Ye, S. Roy, M. Godjevac, and S. Baldi, “A switching control perspective on the offshore construction scenario of heavy-lift vessels,” *IEEE Transactions on Control Systems Technology*, pp. 1–8, 2020.